

Archive ouverte UNIGE

https://archive-ouverte.unige.ch

Chapitre d'actes

2004

Accepted version

Open Access

This is an author manuscript post-peer-reviewing (accepted version) of the original publication. The layout of the published version may differ .

Regularized two-step brain activity reconstruction from spatio-temporal EEG data

Alecu, Teodor; Voloshynovskyy, Svyatoslav; Pun, Thierry

How to cite

ALECU, Teodor, VOLOSHYNOVSKYY, Svyatoslav, PUN, Thierry. Regularized two-step brain activity reconstruction from spatio-temporal EEG data. In: Image Reconstruction from Incomplete Data III, SPIE International Symposium on Optical Science and Technology. Denver (USA). [s.l.]: [s.n.], 2004. (SPIE proceedings) doi: 10.1117/12.556293

This publication URL: https://archive-ouverte.unige.ch/unige:47710

Publication DOI: <u>10.1117/12.556293</u>

© This document is protected by copyright. Please refer to copyright holder(s) for terms of use.

Regularized two-step brain activity reconstruction from spatiotemporal EEG data

Teodor Iulian Alecu, Sviatoslav Voloshynovskiy and Thierry Pun Computer Vision and Multimedia Laboratory, 24 Rue Général Dufour, 1211 Geneva 4, Switzerland Teodor.Alecu@cui.unige.ch

ABSTRACT

We are aiming at using EEG source localization in the framework of a Brain Computer Interface project. We propose here a new reconstruction procedure, targeting source (or equivalently mental task) differentiation.

EEG data can be thought of as a collection of time continuous streams from sparse locations. The measured electric potential on one electrode is the result of the superposition of synchronized synaptic activity from sources in all the brain volume. Consequently, the EEG inverse problem is a highly underdetermined (and ill-posed) problem. Moreover, each source contribution is linear with respect to its amplitude but non-linear with respect to its localization and orientation. In order to overcome these drawbacks we propose a novel two-step inversion procedure.

The solution is based on a double scale division of the solution space. The first step uses a coarse discretization and has the sole purpose of globally identifying the active regions, via a sparse approximation algorithm.

The second step is applied only on the retained regions and makes use of a fine discretization of the space, aiming at detailing the brain activity. The local configuration of sources is recovered using an iterative stochastic estimator with adaptive joint minimum energy and directional consistency constraints.

Keywords: Brain Computer Interface, EEG, source localization, inverse problem, regularization, stochastical estimators

1. INTRODUCTION

Solving the EEG inverse problem arises in various medical fields as a tool for correct and relevant interpretation of EEG (electroencephalograph) data. The goal is to map back the data measured on the scalp surface to the brain volume, allowing for direct physiological analysis. Unfortunately, for two major reasons, solving the EEG inverse problem is not a straightforward task.

First, and most importantly, the problem is highly underdetermined. Indeed, the EEG data is a distant measurement of the brain activity in an inhomogeneous medium. The measuring system is composed of a number of electrodes which may vary, roughly, between 16 and 256, which sample more or less regularly the scalp surface. Thus, the 3D electric field is measured on a discrete set of points on a 2D surface. The Laplace equation insures uniqueness of the source distribution for a given electric field, but this property is ineffective because of the EEG data incompleteness. Moreover, the scalp-air interface provokes an important smearing effect which inherently reduces the relative differences between potential fields distributions. We are therefore facing the task of volume source reconstruction from sparse measurements of a low-pass filtered 2D electric field distribution.

Secondly, the EEG data is not only incomplete, attenuated and smeared but also exhibits high noise values of very differing nature, to name a few, electrode noise, eye blinking artifacts and 50 (or 60) Hz noise. This may not only cover the brain activity, but also mislead the reconstruction by transforming one potential field into another.

We concentrate in this article on how to properly constrain the EEG inverse problem in order to achieve robust data reconstruction, in spite of the above obstacles.

EEG measurement has one significant advantage over its complement, MEG (magnetoencephalography), that is its high temporal resolution, which enables temporal redundancy of source data. Most of the state of the art solutions tend to ignore the temporal information, concentrating on spatial modeling, mostly because of the computational complexity required and of the absence of any explicit quantifiable priors on temporal brain activity behavior. We introduce in this paper (Section 6) implicit temporal regularization induced by structural constraints, made possible by the aforementioned redundancy. We will thus solve a spatiotemporal problem, using overlapping time-windows. This will be our first aid in overcoming the noise and underdetermination drawbacks.

The second is derived out of the observation that the relevant information we are looking for is usually confined in a reduced portion of the brain volume. This is the case for our main targeted application, Brain Computer Interface, where the main goal is discerning between different mental states of a user. This is the case as well for numerous medical applications, e.g. epileptic seizure localization. Thus, instead of full space reconstruction, we can fully reconstruct a well-selected subvolume only and approximate elsewhere. This leads us to a two-step solution (Section 7) based on a double scale division of the solution space. The first step uses a coarse discretization and has the sole purpose of globally identifying the active regions, while the second step is applied only on the retained regions and makes use of a fine discretization of the space, aiming at detailing the brain activity.

We begin this paper by describing the physical model at the basis of our research (Section 2). We continue with the mathematical formulation of the EEG inverse problem in Section 3 and the description of our solution framework in Section 4. Sections 5, 6 and 7 define the constraints which we will impose on our EEG inverse solution. Section 8 is dedicated to the presentation of qualitative and quantitative results, compared with some state of the art techniques.

2. PHYSICAL MODEL: FORWARD PROBLEM

We discuss in this section the physical relationships between a given brain source activity and the corresponding EEG, as we need to solve the forward problem before attacking the inverse one.

2.1. EEG origin

The origin of the scalp measured electric activity of the brain lies in the synaptic activity of neurons. However, the identification of an appropriate model for source modeling is not a trivial problem. Consider a multipolar decomposition of source configurations. Theoretically, any term of such decomposition can be expressed as a combination of monopole sources of smaller size, but it is obvious that there are no independent electric charges present in the brain. We need to investigate the underlying process of synaptic activity.

The propagation of neuronal excitations is done through axon potentials, which exhibit quadripolar fields. The intensity of these local fields is however too weak to explain the EEG data. The current widely accepted explanation [1] relies on the synchronization of activities of multiple neurons at the dendrite-dendrite level. The neuron to neuron excitation transmission at dendrite level can be modeled, from the physical point of view, as an accumulation of charges (ions), and thus, as a current dipole. Synchronization of excitations leads to measurable electric fields, integrating all the smaller currents into an observable one. This explains the adoption of the dipole model as the brain source model in all the EEG community. Moreover, while it is not obvious to justify the dipole source character at a larger scale, any higher order multipole can be obtained through finer scale dipole configurations, albeit with an increase in complexity.

2.2. Forward problem

It is quite easy to express the field of a current dipole in a homogeneous infinite conductive volume. The human head is however neither homogeneous nor infinite. The most accurate methods for computing the EEG corresponding to one dipole rely on realistic head models and finite or boundary elements techniques ([2], [3] and [4]). The complexity of these methods is very high, and the computations should be repeated for each different subject. Our goal is to compare and validate inversion methods, and for that purpose the use of a generic spherical models is more than sufficient, also allowing easy benchmarking. This explains the large use of these models in researches related to this problem.

We use in this paper a 4-layer spherical head model as described by Zhang in his paper [5], under the name of Stok1 head. We also employ the analytical expansion which is presented therein, which can be written in simplified form as (for a unit radius sphere with isotropic layers):

$$V = \frac{1}{4\pi\sigma_{scalp}} \sum_{n} \frac{2n+1}{n} R_0^{n-1} f_n \left(nD_r P_n \left(\cos \gamma \right) + \cos \left(\beta \right) D_r P_n^1 \left(\cos \gamma \right) \right), \tag{1}$$

where V is the measured scalp potential, D_r and D_t represent the radial and the tangential components of the dipole, R_θ stands for the dipole's eccentricity (Figure 1, from [5]), P_n and P_n^I are the Legendre and respectively the associated Legendre polynomials, σ_{scalp} is the scalp conductivity, β and γ are dipole-electrode geometry related parameters and the f_n functions are also linked with the layers parameterization. V is, of course, the field potential at the electrode position.

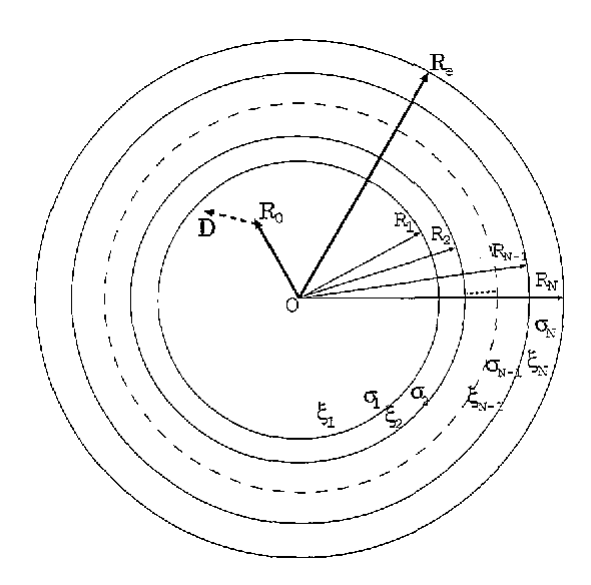


Figure 1. N-layer spherical model

For more details refer to Zhang's paper [5], which also describes a fast method for approximation, now rendered obsolete by the increase in processors' speed.

3. PROBLEM FORMULATION

We have considered in the previous section the relationship between one dipole source and the corresponding scalp measurements. In practice we need to estimate brain activity over the full gray matter volume. We can write:

$$V = \int_{r_0} l(r_0) \vec{j}(r_0) \tag{2}$$

l in equation (2) is the lead-field operator defined according to the Zhang formula (1) as the potential field at the electrodes for a unitary dipole at position r_0 , which spans the gray matter volume, and \vec{j} is the source current density. One needs to model the above integral in discrete form in order to perform computer assisted inversion.

The first possibility is to restrain the number of sources to a finite and preferably small value. This way, the integral in (2) reduces to a finite sum:

$$V = \sum_{1 \le i \le N_s} l(r_0^i) \vec{j}(r_0^i)$$
(3)

This type of solution is considered in numerous papers, such as [6], [7]. The main drawback consists in the nonlinearity of the lead-field operator with respect to the source position, which imposes the use of nonlinear optimization techniques, reputedly slow. Also, the source reconstruction necessarily yields nonrealistic Dirac-like sources.

We prefer to use a distributed modelization of the brain volume [2], which transforms (2) into a linear equation. The gray matter volume is discretized into voxels (volume pixels) of fixed positions, which should be small enough to preserve the coherence of the lead-field inside one voxel. Given that the lead-field is linear with respect to the source amplitude (1), we simply have (with L the lead-field matrix containing on rows the l corresponding to each voxel):

$$V = LJ \tag{4}$$

It is necessary to emphasize that the number of voxels is much higher than the number of electrodes. We have traded the nonlinearity issue with an underdetermination issue. However, this distributed model not only allows for fast linear operations, but also permits realistic reconstruction results (continuous spatial activity as opposed to Dirac-like).

We complete our formulation with the inclusion of the temporal dimension (i as the time sample) and of an additive noise term n. Finally:

$$V^{i} = LJ^{i} + n^{i} \tag{5}$$

Both in equations (4) and (5) L is the lead-field matrix associated with the electrodes and the voxels obtained through volume discretization, and J is a column vector containing the current source amplitudes in each voxel. Since a current dipole is a vector quantity, the size of the matrices involved in equation (5) are:

 $V, n \Rightarrow 1 \times N$, with N the number of electrodes

 $J \Rightarrow 1 \times 3M$, with M the number of voxels

$$L \Rightarrow N \times 3M$$

Typically M is of the order of thousands and N ranges from 16 to 256. We use in the results section a simulated system of 4024 voxels and 123 electrodes.

From this point on, any reference to the EEG inverse problem in this paper should be interpreted as a reference to equation (5), as we base our analysis on the linear distributed model with additive noise.

4. INVERSION FRAMEWORK

As the EEG inverse problem is a highly underdetermined problem, an infinite number of solutions exist for any EEG measurements. One needs to constrain the inverse solution in order to impose uniqueness and counter ill-posedness. Two main approaches are present in the literature concerning generic inverse problems: deterministic regularization and stochastic estimators.

4.1. Deterministic regularization

This is the approach which is used in the state of the art techniques for the EEG inverse problem (Loreta [10], [14], Laura [12], Focuss [9]). The solutions are based on Tikhonov-like regularization [11], [13], [14], evaluating the current density as:

$$J = \arg\min\left(\left\|V - LJ\right\|^2 + \lambda \left\|WJ\right\|^2\right) \tag{6}$$

The W parameter is a weighting matrix, and λ is a regularization parameter. Loreta actually discards the first term and minimizes the second term over the set of exact solutions, with W the second order derivative operator (Laplacian).

The Laura solution keeps the regularization parameter λ , but no hint is given by the authors as to the setting of this parameter. The weighting matrix W is a more generic high pass filter based on the distance between voxels (which can yield the Laplacian operator). Generally, the solution to the equation (6) is given in the form (with I the identity matrix):

$$J = W^{-1}L'\left(LW^{-1}L' + \lambda I\right)V\tag{7}$$

Notice that one considerable difficulty resides in the inversion of the weighting matrix, because of the sheer size of W. The Focuss solution is somehow more elaborate as it iteratively updates W as the energy of the previous estimate, yielding finally more focused solutions.

None of the above solutions explicitly take into account noise and source modeling, although the form of the regularization functional (L2 norm) implicitly considers Gaussian noise and Gaussian sources. We address these issues in the present paper.

4.2. Spatiotemporal MAP framework

We place our analysis in the framework of stochastic estimators, more precisely MAP estimator. We evaluate J as the maximizing functional of the a posteriori probability:

$$J = \arg\max\left[p(V \mid J)\Box p(J)\right]$$
 (8)

Taking the natural logarithm and inverting the sign:

$$J = \arg\min\left[\Phi_n(V - LJ) + \Phi_J(J)\right]$$

$$\Phi_n(V - LJ) = -\ln p(V | J); \Phi_J(J) = -\ln p(J)$$
(9)

The first term of the functional in (9) is only noise distribution dependent, while the second one is source distribution dependent. Therefore, we can consider separately the noise and source modeling. However, we apply the principle in equation (9) not for a time sample, but for a time window, which requires the probability distributions involved to be treated as spatiotemporal distributions. Their modelization (and implicitly of the regularization functional) is the subject of the following sections

5. NOISE MODELING

Noise definition demands the investigation of both the spatial and temporal characteristics. In this paper we make the assumption of temporally white noise, meaning that noise realization at sample i+1 is independent of the realization at sample i. We do not make any a priori assumptions about the spatial correlations of the noise, as we plan to determine it from the data, but we assume Gaussian probability distribution:

$$p_{n}(n^{i}) = \frac{1}{(2\pi \det(R_{nn}))^{N/2}} \exp^{-\frac{1}{2}(n^{i})^{i}R_{nn}^{-1}n^{i}}$$
(10)

Superscript t in equation (10) stands for transposed, and R_{nn} is the spatial covariance matrix of the data. The Gaussian assumption allows for the first functional term in equation (9) to be quadratic:

$$\Phi_{n}(V - LJ) = \frac{1}{2}(V - LJ)^{t} R_{nn}^{-1}(V - LJ)$$
(11)

We privilege quadratic assumptions (in the absence of confirmed priors) mainly for their low computational cost, as the minimization of quadratic functionals yields closed-form solutions. This is **not** a negligible advantage when considering high-dimensionality problems as the EEG inverse problem. This also explains their wide use in deterministic regularization methods (see previous section). It is also obvious that if R_{nn} is the identity matrix we particularize to the first term of the deterministic functional (6).

5.1. Estimation

In order to estimate the covariance matrix of the data we rely on our previous assumption of temporally whiteness and also on a frequency-band related information. The frequency band of brain signals spreads from 3 to roughly 40-100 Hz (while there can be discussion about the exact value of the upper bound, it is certainly below 100 Hz, and in most medical applications it is set at 30 or 40 Hz), while the sampling frequencies of EEG are usually set at the values of 512 or 1024 Hz. This implies that we have a physiologically out-of-band spectrum ranging from the upper-bound frequency to the Nyquist frequency, which we can use to determine the noise characteristics through the spectral density. The proposed estimation scheme is then (with $n_{outofband}$ the out-of-band noise):

$$n_{outofband} = high _pass \left(EEG _signal, f_{up} \right)$$

$$R_{nn} = \kappa \operatorname{cov}(n_{outofband}) \text{ with } \kappa = \frac{f_s}{f_s - 2f_{up}}$$
(12)

 f_s in equation (12) is the sampling frequency, while f_{up} is the upper physiological frequency. The normalization constant k is imposed by the white noise assumption (we have the same noise spectral density in the physiological band).

6. SOURCE MODELING

We treat in this section the source modeling possibilities and the constraints which can be imposed on the inverse solution from this perspective. We address, as in the previous section, the probability distribution characterization, but also introduce the structural constraints, used for implicit temporal regularization.

6.1. Spatial covariance matrix

As we use a double scale division of the solution space we need to model the probability distributions both at local (fine scaling) and at global (coarse scaling) level. We assume, similarly to the previous section, time independency of the realizations.

6.1.1. Local statistics

We model the prior source distribution locally as Gaussian

$$p_{Ilocal}\left(J^{i}\right) = \frac{1}{\left(2\pi \det\left(R_{JIlocalprior}\right)\right)^{N/2}} \exp^{-\frac{1}{2}\left(J^{i}\right)^{i}R_{JIlocalprior}J^{i}}$$
(13)

Although there are no grounds to claim the validity of this prior, it leads to the classical quadratic term used in deterministic regularization approaches. We actually use it in an iterative fashion, described in section 7, modifying the covariance matrix at each iteration step, which finally yields a non-Gaussian data-dependent distribution.

In [8] we have studied the properties of an EEG electrode system with respect to the single source localization in the framework of quadratic norm based inversion. We use the localization kernel R_{res} as defined therein corresponding to our noise level and convolute it to the covariance matrix $R_{JJocalprior}$ in (13). This way we use the prior knowledge of the system's spatial resolution to estimate collectively sources which can not be separated. Thus we define the blurred covariance matrix R_{JJocal} as:

$$R_{JJlocal} = conv \left(\underbrace{R_{JJlocalprior}}_{\text{prior model}}, R_{res}_{\text{localization PSF}} \right)$$
 (14)

Finally, our second term of the regularization functional in (9) is

$$\Phi_{JJlocal}\left(J\right) = \frac{1}{2}J^{t}R_{JJlocal}^{-1}J\tag{15}$$

We still need to estimate $R_{JJocalprior}$ from the data. The estimation procedure is explained in subsection 6.3. and is used in the framework of the iterative algorithm section 7.

6.1.2. Global statistics

We express the global statistics in similar fashion to the local statistics, without the localization kernel, as we use at this level a coarse discretization of the space, such that the voxels are larger than the width of the localization point spread function. At the global level we have then:

$$R_{JJglobal} = R_{JJglobalprior}$$

$$\Phi_{JJglobal} (J) = \frac{1}{2} J^{t} R_{JJglobal}^{-1} J$$
(16)

We use the same estimation procedure at the global level for $R_{JJelobal}$ as at the local level for $R_{JJocal brior}$.

6.2. Structural constraints

Consider the following set of common knowledge facts about the EEG measurements and brain activity:

- The synaptic pathways do not change over time (at least for the duration of one recording).
- The EEG sampling frequency is considerably higher than the native frequencies of brain signals.

From the above statements we draw the directional consistency principle:

If the duration of an inversion time window is properly chosen, inside that time window the reconstructed dipoles should have the same orientation.

Moreover, the above principle should apply both at local and at global level. We use the above principle as an implicit regularization tool, through the use of the directional consistency measure Γ as a selection criterion in the framework of our iterative algorithm:

$$\Gamma = \frac{1}{T} \sum_{i < T} \frac{J^{i} . J^{i+1}}{\|J^{i}\| \|J^{i+1}\|}$$
(17)

T is the length of the time window.

Now consider a second set of common knowledge facts:

- Discontinuities are natural between neighboring but functionally different brain regions.
- All regions are active, but only a few produce measurable, high intensity fields.
- These regions are mental task related regions.

The above considerations enable our global level **space reduction** approach:

- 1. Partition the brain volume into functionally different regions.
- 2. Select the active brain regions using global priors.
- 3. *Inverse locally in the selected regions.*

Since the inversion is simultaneously performed on several time frames, the space reduction procedure acts as an implicit continuity constraint (same volumes are selected for reconstruction in successive time frames).

6.3. Estimation

We discuss in this subsection the estimation of local and global covariance matrices. As we do not have any prior information about the source position, we use covariance matrices of the form:

$$R_{JJprior} = \varepsilon^2 I \tag{18}$$

In equation (18) I is the identity matrix and ε^2 is a scalar value which needs to be set at the mean energy of the source. As we are considering Gaussian processes we should have:

$$R_{VV} = R_{nn} + \varepsilon^2 L L^t \iff \varepsilon^2 = \left(L L^t\right)^{-1} \left(R_{VV} - R_{nn}\right)$$
(19)

 R_{VV} is the estimated covariance matrix of the data. However, since our ideal modeling is not perfect, the equality (19) will not hold. We can nevertheless estimate ε^2 as:

$$\varepsilon^{2} = \frac{Trace(R_{VV} - R_{nn})}{Trace(LL')}$$
(20)

We can now compare our result with (7) and note that the functionals are identical when particularizing:

$$\varepsilon^2 R_{res} = W^{-1}$$
$$R_{nn} = \lambda I$$

The benefit of our modeling is that not only it is derived from a generic framework, allowing for different types of parameterization, but also that it includes automatic data-driven estimation of regularization parameters.

7. RECONSTRUCTION SCHEME

We synthesize in this section the previously described conjectures and modeling work by defining the reconstruction procedure which encompasses them. We begin by the description of the core algorithm, iterative Gaussian based, and continue with the full regularization scheme.

7.1. Gaussian Iterative algorithm

obtain an estimate of the current density by:

Most of our modeling is based on Gaussian distributions, which allow for closed-form solutions and therefore fast computations, a primary concern for large systems such as ours. True distributions, however, are not usually Gaussian. In order to approximate non-Gaussian source data we propose an iterative algorithm which is at each step Gaussian but whose parameters evolve at each iteration. In the spirit of the previous sections we will proceed by space-reduction. We begin by estimating the noise covariance matrix through the method described in 5.1. We pursue with the computation of the associated resolution kernel and of the mean source energy as described in subsection 6.3. Then we

$$\hat{J} = R_{II} L' \left(L R_{II} L' + R_{mn} \right)^{-1} V \tag{21}$$

Using the current estimate we select for the next iteration a reduced solution space by imposing a relative lower threshold for either the energy of the estimate or for the directional consistency measure, e.g.:

$$\Gamma_{selected} \ge \kappa_{tr} \Gamma_{max}$$
 (22)

 k_{tr} is the relative lower threshold. The pertinence of the selection criterion is a highly influential factor on the success of the procedure, (see section 8). The lower threshold evolves between a minimum and a maximum, increasing at each iteration step. We repeat the estimation-selection couple, updating at each step the mean estimate energy of the sources, until the cumulative probability P_n of the estimated noise (error) is below a certain tolerance *tol*:

$$P_{n}\left(\left\|n\right\|_{R_{xx}} \ge \left\|V - L\hat{J}\right\|_{R_{xx}}\right) < tol$$
(23)

Thus we stop when the predicted error is no longer explained by the noise, which implies that some sources should be localized in the discarded space, and restore the last good estimation. The above stopping criterion holds for regions with low signal-to-noise ratio, where the functional ϕ_n is dominant with respect to ϕ_L . A complete condition for interruption would take into consideration the evolution of the MAP functional (9), but (23) is sufficient in our targeted SNR zone (EEG data typically exhibits SNR below 10 dB).

Two remarks are necessary at this point:

1) It may happen that during the selection procedure the number of retained possible sources drop below the number of electrodes, turning the system into an overdetermined problem. Instead of (21) we need to use the regularized least-square-like solution of MAP problem:

$$\hat{J} = \left(L' R_{m}^{-1} L + R_{ll}^{-1}\right)^{-1} L' R_{m}^{-1} V \tag{24}$$

2) Unlike the classical MAP formulation, two source configurations may produce the same measurement V and error $\|V - L\hat{J}\|_{R_m^{-1}}$. In this case, the source closer to the surface is privileged, as the second term in the regularization functional minimizes $\|\hat{J}\|$. We use then in equations (21) and (24) a normalized (weighted) version of the source covariance matrix:

$$(wR_{IJ})_{ij} = \frac{(R_{IJ})_{ij}}{\|L_i\| \|L_i\|}$$
 (25)

In equation (25) L_i and L_j are columns of the lead-field matrix, and wR_{jj} is the weighted source covariance matrix. To summarize the Gaussian iterative algorithm:

- Estimate the noise covariance matrix R_{nn} , (12) compute the resolution kernel R_{res}
- Estimate the mean source energy (20)
- Compute the current source estimate through (21) or (24)
- Stop according to (23) and return the previous result
- Else select the new solution space (22) and loop back to energy estimation

7.2. Full scheme

We base our full reconstruction scheme (Figure 2) on the constraints defined in the previous section and on the iterative

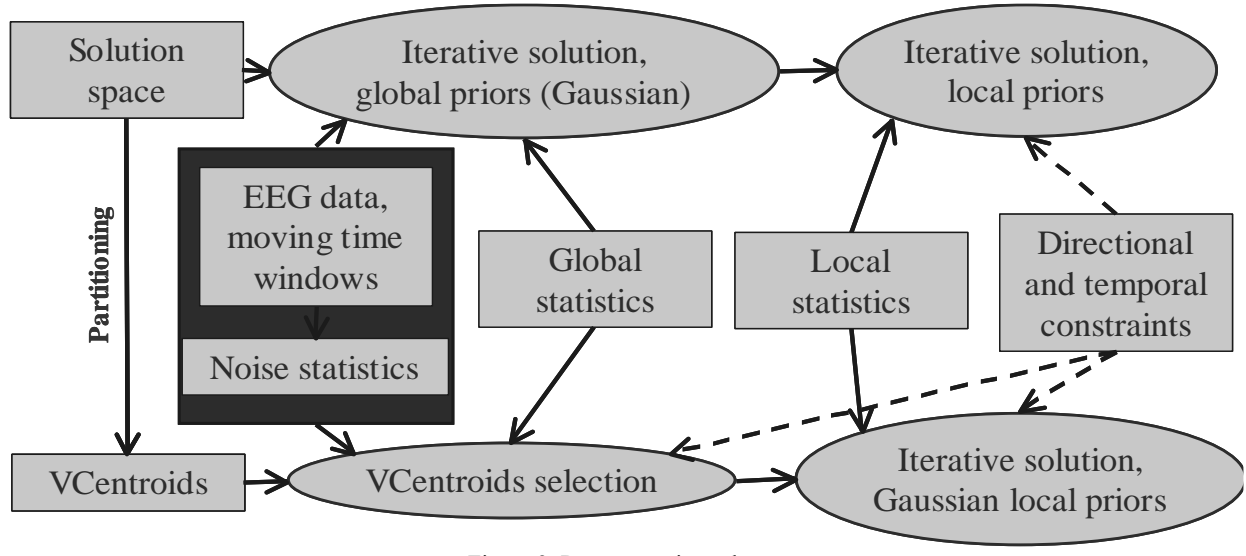


Figure 2. Reconstruction scheme

Gaussian algorithm described in subsection 7.1. The upper branch in Figure 2 does not make any use of the region partitioning and simply iterates on the initial solution space. The lower branch operates first on the geometrical centres (VCentroids) of the different regions defined, using global statistics, and then only on the volumes corresponding to the selected VCentroids, using local statistics. At both levels we use the same iterative algorithm, but differently parameterized. Abrupt increases of the minimum selection threshold k_{tr} are fitted for focalized solutions (generally used at global level), while smooth increases or stagnation correspond to smooth source distributions (normally at local

level). We are in this manner able to apply smoother or sharper priors while using the same core algorithm with different settings.

Our two-step technique not only reduces the underdetermination of the system (5), but also authorizes the use of more memory demanding techniques such as explicit temporal regularization. This is however beyond the scope of the present paper.

8. RESULTS

We used a simulated environment for testing our reconstruction scheme. We concentrated on the lower branch of Figure 2 and performed statistical analysis with random sources in the presence of additive noise, investigating mainly localization errors, both for principal and secondary (lower energy) sources. We also present qualitative results (reconstruction images) to exemplify our technique.

8.1. Simulation setup

On a simulated 4-layer spherical head of unit radius (see section 2) we superposed an 123 electrode system in Neuroscan spherical positions. 4024 cubic voxels¹ of edge length 0.06 (unitless, corresponds to roughly 7mm for an average human head) were used to discretize the gray-matter volume (solution space). Neighboring voxels were further regrouped into 41 cubic regions, yielding a mean of 100 voxels per region.

We then placed randomly one, two and three-dipoles configurations in the brain volume, generating half-a-second long oscillatory sequences of source data, with random frequencies ranging from 3 to 40 Hz and sampled at $f_s = 512Hz$.

After computing the ideal potential measurements at the electrodes' positions we added white Gaussian noise with corresponding SNR ranging from 0 to 30 dB and performed the inversion procedure as described in section 7.

For each SNR value and configuration type (one, two or three dipoles) we repeated the above procedure for $N_{trials} = 100$ times, generating a total number of 4800 reconstructions (16 SNR values, 3 configuration types), as we only reconstructed the data for the first time-window. The length N_T of the time window was set in concordance with the Nyquist frequency:

$$N_T = floor \left(\frac{f_s}{2f_{up}} \right) \tag{26}$$

In our case the corresponding value is 6. Also, the *tol* parameter was set to 0.1.

8.2 Analysis

We base our analysis on the definition of the mass-center r_{mass} of the reconstructed sources:

$$r_{mass} = \frac{\sum ||A(r)|| r}{\sum ||A(r)||}$$
 (27)

A(r) represents the amplitude of the estimated dipole at position r. We compare the position of this mass-center with the position of the original source in order to obtain the localization error Δr_{err} :

$$\Delta r_{err} = r_{mass} - r_0 \tag{28}$$

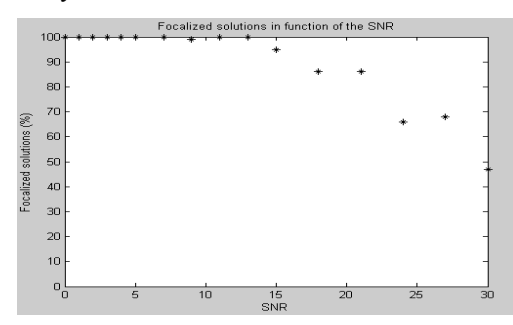
For the case of double or triple dipole configurations we begin by dividing the solution space in a number of subvolumes equal to the number of original sources, and then compute the center of mass for each of the subvolumes. The subvolume selection for each solution point is done according to (29):

$$i_{subvolume}(r) = \arg\min \frac{\|r - r_{0i}\|}{\|A_i\|}$$
(29)

We also denote as the principal source the original source with the highest amplitude, as the (first) secondary source the second amplitude source and as the second secondary source the lowest amplitude source in the case of three dipoles configurations.

¹ The corresponding positions were obtained courtesy of Rolando Grave de Peralta and Sara Gonzales-Andino from the "Hopital Universitaire de Geneve"

As we mentioned in section 7, the stopping criterion (23) is not well suited for low noise regimes, and tends to produce early stops above the SNR value of 18. We call focalized solutions the reconstructions where at least one step of space reduction has been successful (number of retained points smaller than 4024). The percentage of focalized solutions is of approximately 100% from 0 to 15 dB and tends to decrease towards 30 dB (Figure 3, left).



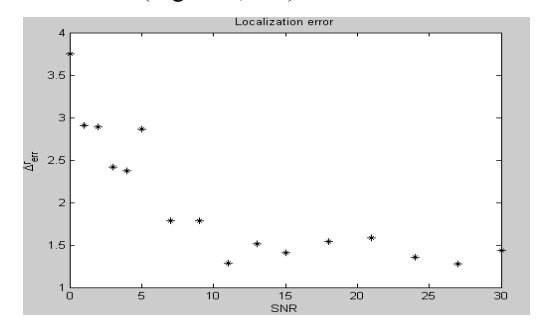


Figure 3. Influence of the stopping criterion on focalization (left) and single source localization error (in voxels, right)

The horizontal axis is the SNR expressed in dB

We retain for computation purposes only the focalized solutions, as no iteration is performed on the non-focalized ones. The first obvious measure is the standard deviation of the single source localization error (Figure 3, right). The values decrease from roughly 3-4 voxels around 0 dB to 1.5 voxels at 10 dB and remain constant until the 30 dB limit. Notice that an error of 4 voxels at 0dB (where the noise power equals the signal power) represents an error volume of only, roughly, 1.5% of the full brain volume. More interestingly, the distribution of these errors presents a very large percentage of small errors and a few outliers which negatively influences the values in Figure 3. This brings us to a very common measure in the EEG inverse problem community, the exact localization and distribution of errors. More specifically we look at the cumulative distribution at the exact localization (<1voxel), one voxel ([1-2) voxels) and two voxel ([2-3) voxels) errors limits.

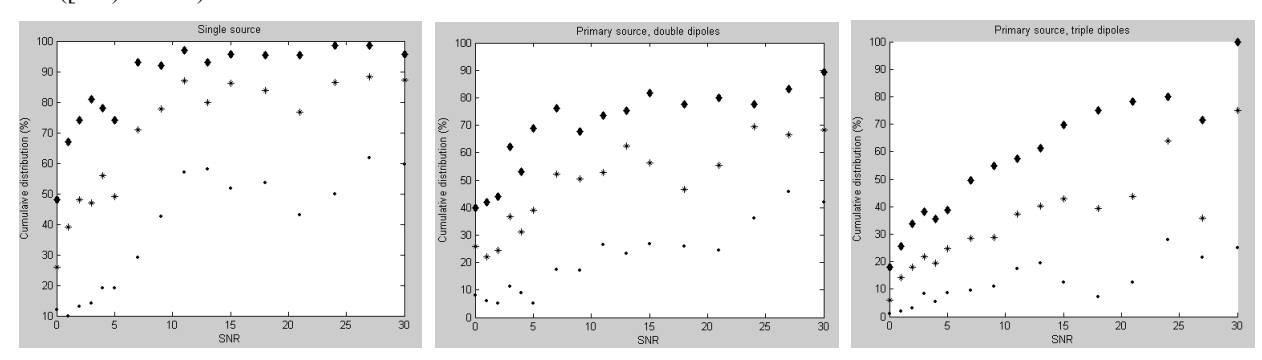


Figure 4. Primary source localization cumulative distribution.

Left: results for singe source configurations. Middle: primary source, double dipoles. Right: primary source, triple dipoles. Points represent exact localization values, stars one voxel errors and diamonds two voxel errors

Unfortunately there are no real studies in the presence of noise, as usually authors test their general purpose methods (Laura, Loreta) in noise free situations and only for single source configurations. However, from Figure 4, our method outperforms both Laura and Loreta (tested without noise in [12]) from the 9dB line and above, when comparing voxel errors (moreover their reported edge length is more than double 0.136 with respect to 0.06). Considering the voxel size, our method yields comparable results even with the EPIFOCUS method, described in the same paper [12], which is specifically designed for single source localization (projective method which explicitly assumes the presence of only one source). Notice that our method is able to recover the primary source even in more complex configurations comprising two or three dipoles (Figure 4).

Figure 5 illustrates the recovery of secondary sources. Although the performance is quite low in the high noise regimes, the secondary sources are generally identified in more than 50% of the simulations at 10 dB and 80% at 30 dB (left and middle). Even the second secondary source (right) is recovered in roughly 50% of the cases in the range 15-30 dB.

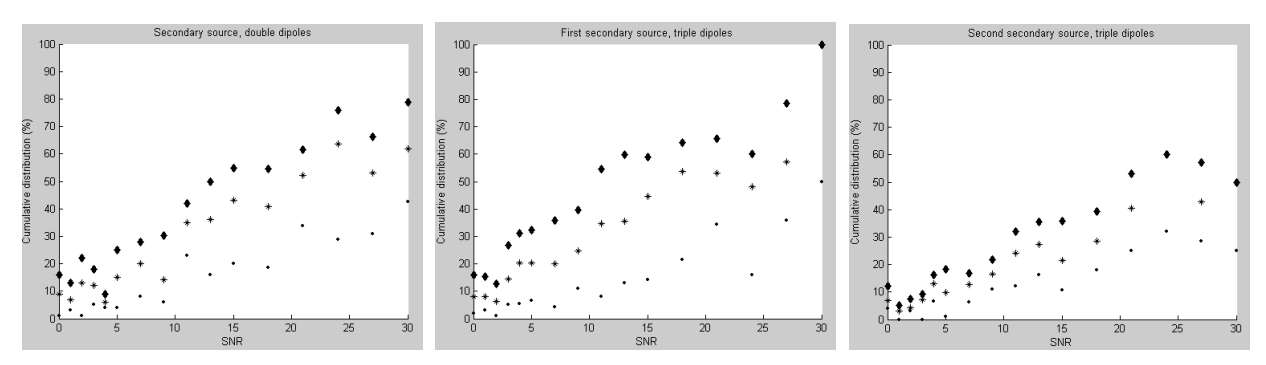


Figure 5. Secondary source localization cumulative distribution.

The abovementioned rates of success for secondary sources can be improved by use of a local thresholding system instead of the global (22). We finish the results section with an example of typical results at 10 dB noise (Figure 6).

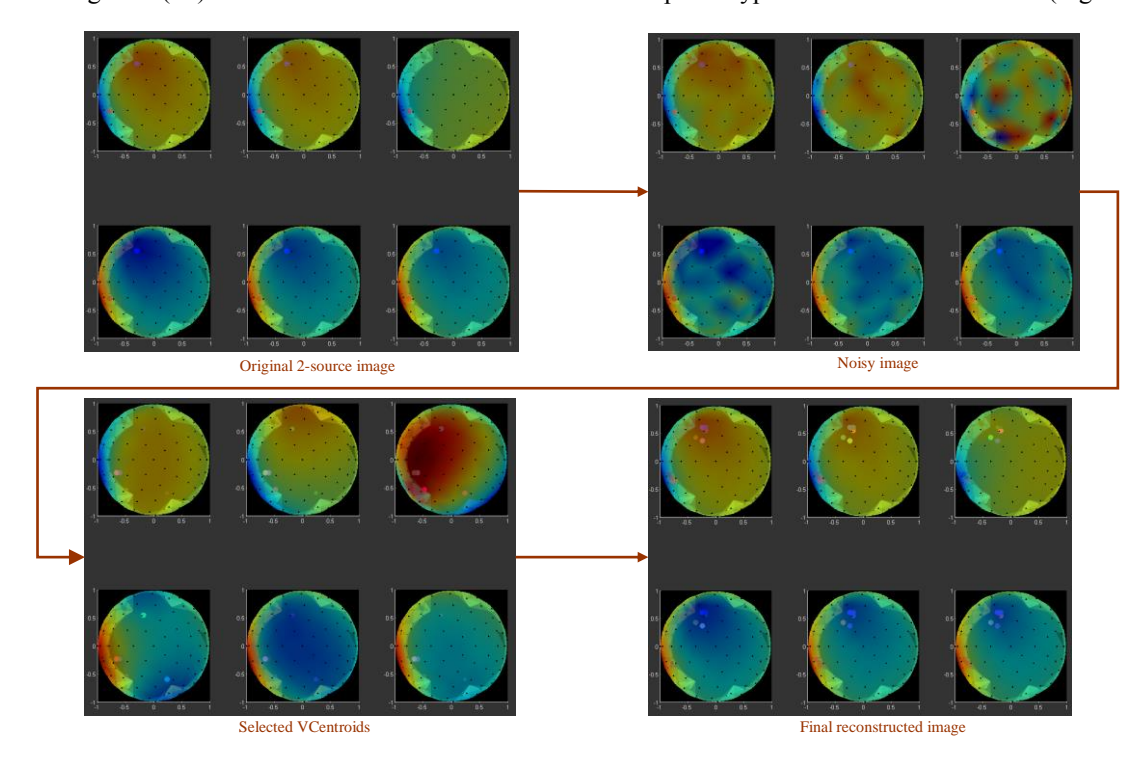


Figure 6. Typical results, 6 frames time-window sample. Time evolution of sources from left to right and then up to down. View top-down, scalp potentials in transparent mode, with red for positive values and blue fro negative.

Dipoles are represented as points, colors indicate orientation.

The correct selection of VCentroids (down-left), although not explaining the data, ensures a fast and reliable solution (down-right). Observe that performing the inverse solution also acts as a denoising tool for the EEG data (compare the scalp potentials from the final image with the original up-left and the noisy version up-right).

9. CONCLUSIONS AND FUTURE WORK

We have proposed in this paper a generalized MAP framework for constraining and solving the EEG inverse problem. We proved that such an approach not only can particularize to classical solutions, but also allows for automatic regularization parameters estimation. Moreover, our reconstruction scheme easily accepts new constraints such as temporal and structural priors. We also introduced anatomically derived principles, such as the directional consistency

measure and the brain partitioning technique. The results confirm the achievement of our main goal, robustness of reconstruction in noisy conditions.

We intend to continue the refinement of our method by firstly identifying the blocks of our reconstructions scheme (that is to obtain statistics of real data). We are currently performing theoretical studies of the equivalence of our Gaussian iterative algorithm with direct minimization of non-Gaussian functionals, aiming for optimal selection (thresholding) methods, as a functions of the prior data statistics. We also plan of introducing explicit temporal constraints (or equivalently losing the temporal independency assumption), benefiting from our space reduction technique.

Finally we will implement our reconstruction scheme as a feature extraction method in the context of a Brain Computer interface. We need to analyze the possibility of direct online use of the algorithm, or of implicit offline use. We will also use it, coupled with the optimal placement technique from [8] to design application targeted optimal portable (reduced number of electrodes) EEG systems.

ACKNOWLEDGEMENTS

This work is supported in part by the Swiss NCCR (National Centre of Research) IM2 (Interactive Multimodal Information Management, http://www.im2.ch) and the EU Network of Excellence Similar (http://www.similar.cc).

REFERENCES

- 1. P.L. Nunez: "Electric Fields of the Brain, The Neurophysics of EEG", Oxford University Press, New York, 1981.
- 2. J. Malmivuo and R. Plonsey: "Bioelectromagnetism Principles and Applications of Bioelectric and Biomagnetic Fields." Oxford University Press. New York, 1995, 461 p.
- 3. Marino F, Halgren E, Badier JM, Gee M & Nenov VI (1993), "A finite difference model of electric field propagation in the human head: implementation and validation". IEEE Proc NE Bioeng conf 82-85.
- 4. P. H. Schimpf, C. Ramon, and J. Haueisen, "Dipole models for the EEG and MEG," IEEE Transactions on Biomedical Engineering, Vol. 49, No. 5, pp. 409-418, 2002.
- 5. Z. Zhang, "A fast method to compute surface potentials generated by dipoles within multilayer anisotropic spheres", Phys. Med. Biol 40, pp. 335-349, 1995.
- 6. Khosla D., Singh M. and Don M. "Spatio-temporal EEG source localization using simulated annealing" IEEE Trans. Biomed. Eng. 44(11), 1075-1091, 1997.
- 7. Mosher, J.C.; Leahy, R.M.; Lewis, P.S., "EEG and MEG: forward solutions for inverse methods", IEEE Transactions on Biomedical Engineering, Volume: 46 3, March 1999, Page(s): 245 -259.
- 8. T.I. Alecu, S. Voloshynovskiy and T. Pun, "Localization properties of an EEG sensor system: lower bounds and optimality", EUSIPCO 2004, 12th European Signal Processing Conference, Vienna, Austria, September 6-10 2004.
- 9. Gorodnitsky IF, George JS, Rao BD. "Neuromagnetic source imaging with FOCUSS: a recursive weighted minimum norm algorithm". EEG and Clinical Neurophysiol., 95: 231-251, 1995.
- R. D. Pascual-Marqui, C. M. Michel, and D. Lehmann, "Low resolution electromagnetic tomography: a new method to localize electrical activity in the brain", Int. J. Psychophysiol. 18, pp. 49–65, 1994.
 A. K. Liu, A. M. Dale, and J. W. Belliveau, "Monte Carlo Simulation Studies of EEG and MEG Localization
- 11. A. K. Liu, A. M. Dale, and J. W. Belliveau, "Monte Carlo Simulation Studies of EEG and MEG Localization Accuracy", Human Brain Mapping 16, pp. 47–62, 2002.
- 12. R. Grave de Peralta-Menendez, S. L. Gonzalez-Andino, "Comparison of Algorithms for the Localization of Focal Sources: Evaluation with simulated data and analysis of experimental data". IJBEM vol. 4, number 1, 2002.
- 13. De Peralta-Menendez RG, Gonzalez-Andino SL: "A critical analysis of linear inverse solutions to the neuroelectromagnetic inverse problem". IEEE Transactions on Biomedical Engineering 45: 440-448, 1998
- 14. Pascual-Marqui RD: "Review of methods for solving the EEG inverse problem". International Journal of Bioelectromagnetism 1: 75-86, 1999.